Piezo1-mediated microtubule destabilisation promotes extracellular matrix rigidity induced smooth muscle cell hypertrophy

Robert T. Johnson[1+], Sultan Ahmed[1], Finn Wostear[1], Reesha Solanki[1], Chris J. Morris[1,2], Stefan Bidula[1] and Derek T. Warren[1+]

[1] School of Pharmacy, University of East Anglia, Norwich Research Park, Norwich, United Kingdom.

[2] School of Pharmacy, University College London, London, United Kingdom.

[+] Corresponding Author(s): Dr. Robert Johnson (robert.johnson@uea.ac.uk) & Dr. Derek Warren (derek.warren@uea.ac.uk)

School of Pharmacy, University of East Anglia, Norwich Research Park, Norwich, Norfolk, UK, NR4 7TJ

ORCiD IDs: RTJ (https://orcid.org/0000-0003-3618-238X)

FW (https://orcid.org/0009-0003-0703-8917)

CJM (https://orcid.org/0000-0002-7703-4474)

SB (https://orcid.org/0000-0002-3790-7138)

DTW (https://orcid.org/0000-0003-0346-7450)

Running Title: Microtubules regulate smooth muscle cell hypertrophy

Word Count: 3,633

Author Contributions: RTJ, SA, FW and RS were responsible for performing experiments and analysing data. DTW analysed data. RTJ, CJM, SB and DTW were involved in the conceptualisation of the study. CJM and SB reviewed and edited this manuscript. RTJ and DTW were responsible for the design, writing and editing of this manuscript.

Acknowledgements: This work was funded by a Biotechnology and Biological Sciences Research Council Research Grant (BB/T007699/1) and a British Heart Foundation PhD Studentship (FS/17/32/32916) awarded to DTW and a UKRI Biotechnology and Biological Sciences Research Council Norwich Research Park Doctoral Training Partnership PhD Studentship awarded to FW.

Conflict of Interests: The authors declare that the research was conducted in the absence of any commercial or financial relationships that could be construed as a potential conflict of interest.

Data Availability: The data that support the findings of this study are available from the corresponding author upon reasonable request.

Abstract

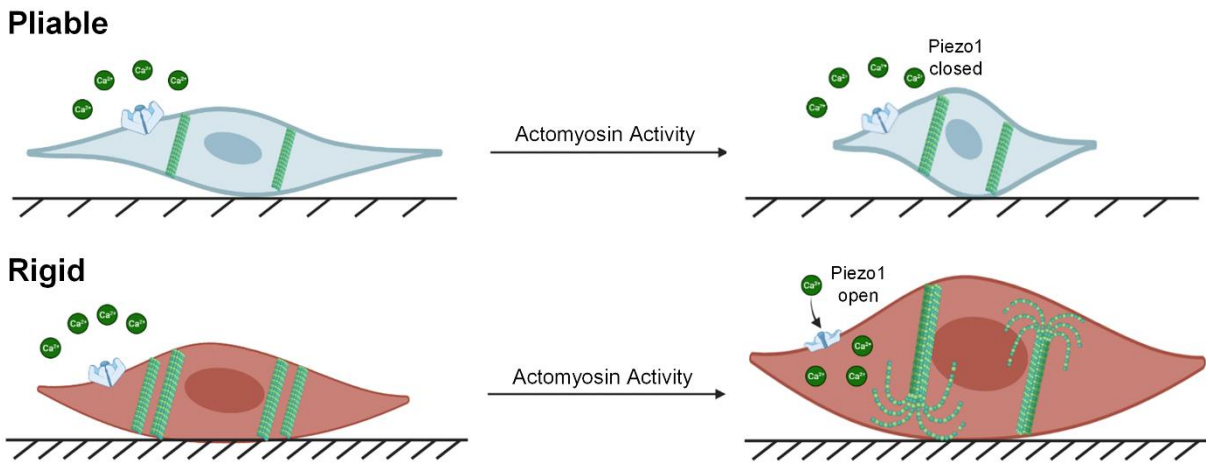

Graphical Abstract

Background and Purpose: Decreased aortic compliance is a precursor to numerous cardiovascular diseases. Compliance is regulated by the rigidity of the aortic wall and the vascular smooth muscle cells (VSMCs) within it. Extracellular matrix stiffening, observed during ageing, reduces compliance and contributes to hypertension. In response to increased rigidity, VSMCs generate enhanced contractile forces that result in VSMC stiffening and a further reduction in compliance. Due to a lack of suitable *in vitro* models, the mechanisms driving VSMC response to matrix rigidity remain poorly defined.

Experimental Approach: Human aortic VSMCs were seeded onto polyacrylamide hydrogels whose rigidity mimicked either healthy or aged/diseased aortae. VSMC response to contractile agonist stimulation was measured through changes in cell area and volume. VSMCs were pre-treated with pharmacological agents prior to agonist stimulation to identify regulators of VSMC hypertrophy.

Key Results: VSMCs undergo a differential response to contractile agonist stimulation based on matrix rigidity. On pliable matrices, VSMCs contract, decreasing in cell area. Meanwhile, on rigid matrices VSMCs undergo a hypertrophic response, increasing in area and volume. Piezo1 mediated calcium influx drives VSMC hypertrophy by promoting microtubule destabilisation. Pharmacological stabilisation of microtubules or blocking calcium influx prevented VSMC hypertrophy on rigid matrices whilst maintaining contractility on pliable matrices.

Conclusions and Implications: In response to extracellular matrix rigidity, VSMCs undergo a hypertrophic response driven by piezo1-mediated microtubule destabilisation. Pharmacological targeting of this response blocks matrix rigidity induced VSMC hypertrophy whilst VSMC contractility on healthy mimicking matrices is unimpeded. Through delineating this rigidity-induced mechanism, we identify novel targets whose pharmacological inhibition may prove beneficial against VSMC-driven cardiovascular disease.

1. Introduction

Aortic compliance describes the ability of the aorta to change shape in response to changes in blood pressure. Maintaining aortic compliance is essential for cardiovascular (CV) health and decreased aortic compliance is a major risk factor associated with a variety of age-related CV diseases (Glasser et al., 1997; Mitchell et al., 2010; Lacolley et al., 2020). Clinical measurements of aortic compliance, using pulse wave velocity, identify that reduced compliance is associated with increased CV mortality (Safar et al., 2002; Zhong et al., 2018; Sequí-Domínguez et al., 2020). The rigidity of the aortic wall is a major contributor to aortic compliance. In the healthy aortic wall, rigidity and compliance are determined by the balance between extracellular elastic fibres, including elastin, which provides pliability, and non-elastic extracellular matrix (ECM) components, including collagen-I, that provides tensile strength to the aortic wall (Tsamis et al., 2013). However, during ageing and CV disease, elastic-fibres degrade, and collagen-I accumulates. These ECM changes increase the rigidity of the aortic wall and decrease aortic compliance (Ahmed and Warren, 2018).

Vascular tone is regulated by the contraction of vascular smooth muscle cells (VSMCs), the predominant cell type within the aortic wall (Leloup et al., 2019). These mechanosensitive cells generate actomyosin-derived forces, with force production increasing as ECM rigidity increases (Petit et al., 2019; Sanyour et al., 2019; Johnson et al., 2021). Enhanced actomyosin force generation increases VSMC stiffness and in turn contributes to increased aortic wall rigidity and reduced aortic compliance observed in ageing and CV disease (Qiu et al., 2010; Sehgel et al., 2015b; Lacolley et al., 2017). In healthy aortae, wall rigidity and compliance are a balance between ECM rigidity and VSMC stiffness (Johnson et al., 2021). However, this balance is disrupted in ageing and CV disease, resulting in VSMC dysfunction (Sazonova et al., 2011; Lacolley et al., 2017). For example, in hypertension, aortic stiffness increases as a result of enhanced ECM rigidity and VSMC hypertrophy, a process through which cell mass increases without a corresponding increase in cell number (Owens and Schwartz, 1983; Rizzoni et al., 2000; Zhang et al., 2005; Schiffrin, 2012; Sehgel et al., 2013). VSMC hypertrophy increases aortic wall thickness and rigidity, resulting in reducing aortic compliance (Zieman et al., 2005; Hayashi and Naiki, 2009; Sehgel et al., 2015a). However, mechanisms driving VSMC hypertrophy remain poorly defined.

In response to matrix rigidity, ECM adhesions activate the Rho/ROCK signalling pathway, resulting in actin polymerisation and myosin light chain phosphorylation, that in turn enhance actomyosin activity (Ahmed and Warren, 2018). In other cell types, actomyosin activity and actin cytoskeleton reorganisation in response to ECM rigidity have been shown to activate stretch activated ion channels (SACs) (Kobayashi and Sokabe, 2010; Nourse and Pathak, 2017). SAC activation enables mechanical stimuli to be converted into biochemical responses through mediating the diffusion of ions, including calcium, across the cell membrane (Kobayashi and Sokabe, 2010). Whether VSMCs possess a similar response to ECM rigidity remains unknown, however, VSMCs possess numerous stretch activated ion channels including piezo1 and members of the TRP (transient receptor potential) family (Lowis et al., 2023). In normal physiology, these channels are activated transiently by blood flow derived stretching of the aortic wall (Liu and Lin, 2022). This stimulates VSMC contraction as a result

of calcium ion influx. These SACs are also reported to contribute to VSMC dysfunction, with piezo1 implicated in atherosclerosis and abdominal aortic aneurysm induced vascular remodelling (Qian et al., 2022; Yin et al., 2022). Whether SACs, including piezo1, are involved in VSMC hypertrophy and the mechanisms by which they drive VSMC dysfunction remain unknown.

Investigating the cellular response to matrix rigidity requires us to move away from the use of tissue culture plastic and glass, materials whose stiffness is around a thousand times greater than that of a healthy aorta (Minaisah et al., 2016). The rigidity of the aortic wall, known as its Young's modulus (measured in kilopascals (kPa)), has been experimentally determined using atomic force microscopy (Hayenga et al., 2011; Tracqui et al., 2011). In this study, we utilised polyacrylamide hydrogels, substrates that can be fabricated to the same rigidity as that of a healthy or diseased aorta (Hayenga et al., 2011; Tracqui et al., 2011; Minaisah et al., 2016; Rezvani-Sharif et al., 2019). We identify that enhanced ECM rigidity promotes VSMCs to undergo hypertrophy following contractile agonist stimulation. VSMC hypertrophy is driven by piezo1-mediated microtubule instability. Finally, pharmacological stabilisation of microtubules, or inhibition of piezo1 prevented ECM rigidity induced VSMC hypertrophy whilst leaving VSMC contractility on healthy mimicking substrates unimpeded.

2. Methods

2.1 Polyacrylamide Hydrogel Preparation

Hydrogels were prepared as described previously (Minaisah et al., 2016). Glass coverslips were activated by treating with (3-Aminopropyl)triethoxysilane for 2 minutes, washed 3x in dH_2O, then fixed in 0.5% glutaraldehyde for 40 minutes. After fixation, coverslips were washed and left to air dry overnight. Polyacrylamide hydrogel buffer was comprised as follows: 12 kPa – 7.5% acrylamide, 0.15% bis-acrylamide in dH_2O; 72 kPa – 10% acrylamide, 0.5% bis-acrylamide in dH_2O. To prepare hydrogels for fabrication, the appropriate volume of buffer was supplemented with 10% APS (1:100) and TEMED (1:1,000) then placed on a standard microscopy slide and covered by an activated coverslip (13 mm coverslips required 30 µl of supplemented buffer; 33 mm coverslips used 50 µl). Once set, the hydrogels were washed 3x in dH_2O to remove any unpolymerized acrylamide, crosslinked with sulfo-SANPAH (1:3,000) under UV illumination (365 nm) for 5 minutes, then functionalised with collagen I (0.1 mg/ml) for 10 minutes at room temperature. Hydrogel stiffnesses have previously been confirmed using a JPK Nanowizrd-3 atomic force microscope (Porter et al., 2020).

2.2 Vascular Smooth Muscle Cell Culture

Human adult aortic VSMCs were purchased from Cell Applications Inc. (354-05a). Standard VSMC culture (passages 3-9) was performed as previously described (Ragnauth et al., 2010; Warren et al., 2015). VSMCs were seeded onto polyacrylamide hydrogels in basal media (Cell Applications Inc Cat# 310-500), 18 hours prior to the beginning of the experiment. Briefly, VSMCs were pre-treated with pharmacological agents for 30 minutes, prior to co-treatment with a contractile agonist for an additional 30 minutes. Experimental specific concentrations are provided in the corresponding figure legends. Please see **Supplementary Table S1** for details of compounds used in this study. Keratinocyte calcium-free basal medium

(Cell Applications Inc Cat#132-500) was used for experiments where VSMCs were cultured in the absence of extracellular calcium.

2.3 Immunofluorescence and VSMC Area/Volume Analysis

Cells were fixed in 4% paraformaldehyde for 10 minutes, permeabilised with 0.5% NP40 for 5 minutes, then blocked with 3% BSA/PBS for 1 hour. Primary staining against lamin A/C (1:200) (Sigma-Aldrich Cat# SAB4200236, RRID:AB_10743057) was performed overnight at 4 °C in 3% BSA/PBS. Secondary staining was performed using the appropriate Alexa Fluor™ 488 antibody (1:400) (Thermo Fisher Scientific Cat# A-11001, RRID:AB_2534069) in the dark for 2 hours. F-actin was visualised using Rhodamine Phalloidin (1:400) (Thermo Fisher Scientific Cat# R145). Images were captured at 20x magnification using a Zeiss LSM980-Airyscan confocal microscope. Cell area and volume was measured using FIJI, open-source software (Schindelin et al., 2012; Ahmed et al., 2022)

2.4 Traction Force Microscopy

VSMCs were seeded onto polyacrylamide hydrogels containing 0.5 µm red fluorescent (580/605) FluoSpheres (1:1000) (Invitrogen). Following angiotensin II stimulation (30 minutes), cell lysis was achieved by the addition of 0.5% Triton X-100. Images were captured at 20x magnification before and after lysis at 2-minute intervals using a Zeiss Axio Observer live cell imaging system. Drift was corrected using the ImageJ StackReg plugin and traction force was calculated using the ImageJ FTTC plugin that measured FluoSphere displacement (Tseng et al., 2012). Briefly, bead displacement was measured using the first and last image of the movie sequence. The cell region was determined by overlaying the traction map with the phase image, selecting the cell traction region with an ROI and extracting the traction forces in each pixel using the XY coordinate function in FIJI (Porter et al., 2020; Ahmed et al., 2022).

2.5 Cold-Stable Microtubule Stability Assay

Cold-stable microtubules were identified as per previous studies (Atkinson et al., 2018). Following treatment, cells were placed on ice for 15 minutes before being washed once with PBS and twice with PEM buffer (80 µM PIPES pH 6.8, 1 mM EGTA, 1 mM $MgCl_2$, 0.5% Triton X-100 and 25% (w/v) glycerol) for 3 minutes. Cells were fixed in ice-cold methanol for 20 minutes then blocked with 3% BSA/PBS for 1 hour. Microtubules were visualised by staining for α-tubulin (1:200) (Cell Signalling Technology Cat# 3873, RRID:AB_1904178) whilst cell nuclei were visualised using a DAPI containing mounting media. Images were captured at 40x magnification using a Zeiss AxioPlan 2ie microscope.

2.6 Cell Viability Assay

Cell viability was determined using a RealTime-Glo™ MT Cell Viability Assay, as per manufacturers instructions. Briefly, 5,000 cells per well seeded in a 96-well plate and exposed to a range of drug concentrations for 1 hour. Luminescence was subsequently measured using a Wallac EnVision 2103 Multilabel Reader (PerkinElmer).

2.7 siRNA Knockdown

VSMC siRNA transfection was performed using HiPerFect (Qiagen) as per manufacturer's instructions, the day before cells were seeded onto hydrogels. The next afternoon, cells were seeded onto hydrogels as above, serum was withdrawn overnight to induce quiescence and the next morning VSMCs were stimulated with Angiotensin II (10 µM) for 30 minutes prior to fixation and downstream histochemical analysis.

siRNA #1 – CCGCGTCTTCCTTAGCCATTA

siRNA #2 - CGGCCGCCTCGTGGTCTACAA

2.8 Western Blotting

Western blotting was performed as previously described (Ragnauth et al., 2010). When looking for Piezo1 expression specifically, lysates were run on a TruPAGE precast 4-20% gradient gel (Sigma-Aldrich) at 120 V for 2 hours. Protein was transferred onto PVDF membrane at 30 V for 3 hours prior to the membrane being blocked in 5% milk/TBST. The following antibodies were used: anti-Piezo1 (1:500) (Novus Cat# NBP1-78537, RRID:AB_11003149), anti-GAPDH (1:4000) (Cell Signalling Technology Cat# 2118, RRID:AB_561053) and anti-Rabbit-HRP (1:2000) (Sigma-Aldrich Cat# GENA934, RRID:AB_2722659).

2.9 Statistical Analysis

The data and statistical analysis in this study complies with the recommendations on experimental design and analysis in pharmacology (Curtis et al., 2018). Experiments were performed by one researcher, with a second researcher then performing the microscopy and downstream analysis. Statistical analysis was performed using GraphPad Prism 9.5. Results are presented as mean ± SEM, with individual data points shown. The number of independent repeats performed, and total number of cells analysed per experiment are detailed in the corresponding figure legend. Unpaired Student's t-tests were used for the comparison of two conditions. To compare more than two conditions a one-way ANOVA was performed, with either a Tukey's or Sidak's multiple comparison post-hoc test being performed as appropriate. Concentration-response curves are presented as mean ± SEM plotted on a logarithmic scale. Log(agonist) vs response curves were generated using non-linear regression. Comparisons between concentration ranges on different hydrogel stiffness were performed using a two-way ANOVA followed by Sidak's post-hoc test. Differences between conditions were considered statistically significant when $P < 0.05$.

3. Results

3.1 Matrix rigidity alters isolated smooth muscle cell response to contractile agonist stimulation.

We set out to determine how enhanced matrix rigidity, akin to that of an aged/diseased aortic wall, would affect VSMC response to contractile agonists. Quiescent VSMCs grown on pliable (12 kPa) or rigid (72 kPa) hydrogels were stimulated with increasing concentrations of the contractile agonist angiotensin II. Changes in VSMC area were used as a measure of contractile response (Ahmed et al., 2022). As previously observed, VSMCs on

pliable hydrogels contracted, indicated by a decrease in cell area as angiotensin II concentration increased (**Figure 1a, b & d**) (Ahmed et al., 2022). In contrast, VSMCs seeded on rigid hydrogels failed to contract (**Figure 1a, c & d**). VSMCs seeded on rigid hydrogels were initially smaller than those on pliable hydrogels, yet when exposed to increasing concentrations of angiotensin II, cell area increased (**Figure 1a & d**). Stimulation of VSMCs with increasing concentrations of an alternative contractile agonist, carbachol, again resulted in a differential response whereby VSMC area was reduced on pliable hydrogels but increased on rigid hydrogels (**Figure 1e-h**). Subsequent experiments were performed by stimulating VSMCs with 10 µM of either angiotensin II or carbachol, a concentration which induced maximal area changes on both rigidities of hydrogel.

To confirm that the above changes were specific for receptor activation, we utilised receptor antagonists irbesartan and atropine. Irbesartan antagonises the angiotensin II type 1 receptor, AT1, whilst atropine antagonises acetylcholine receptors thereby blocking the effects of carbachol. Quiescent VSMCs grown on pliable or rigid hydrogels were stimulated with either angiotensin II or carbachol in the presence of an increasing concentration of their respective antagonist. On pliable hydrogels, increasing concentrations of irbesartan or atropine prevented VSMCs from undergoing a contractile response (**Figure 2a, b, e & f**). Likewise, treatment with irbesartan or atropine prevented contractile agonist induced enlargement of VSMCs on rigid hydrogels (**Figure 2a, c, e & g**).

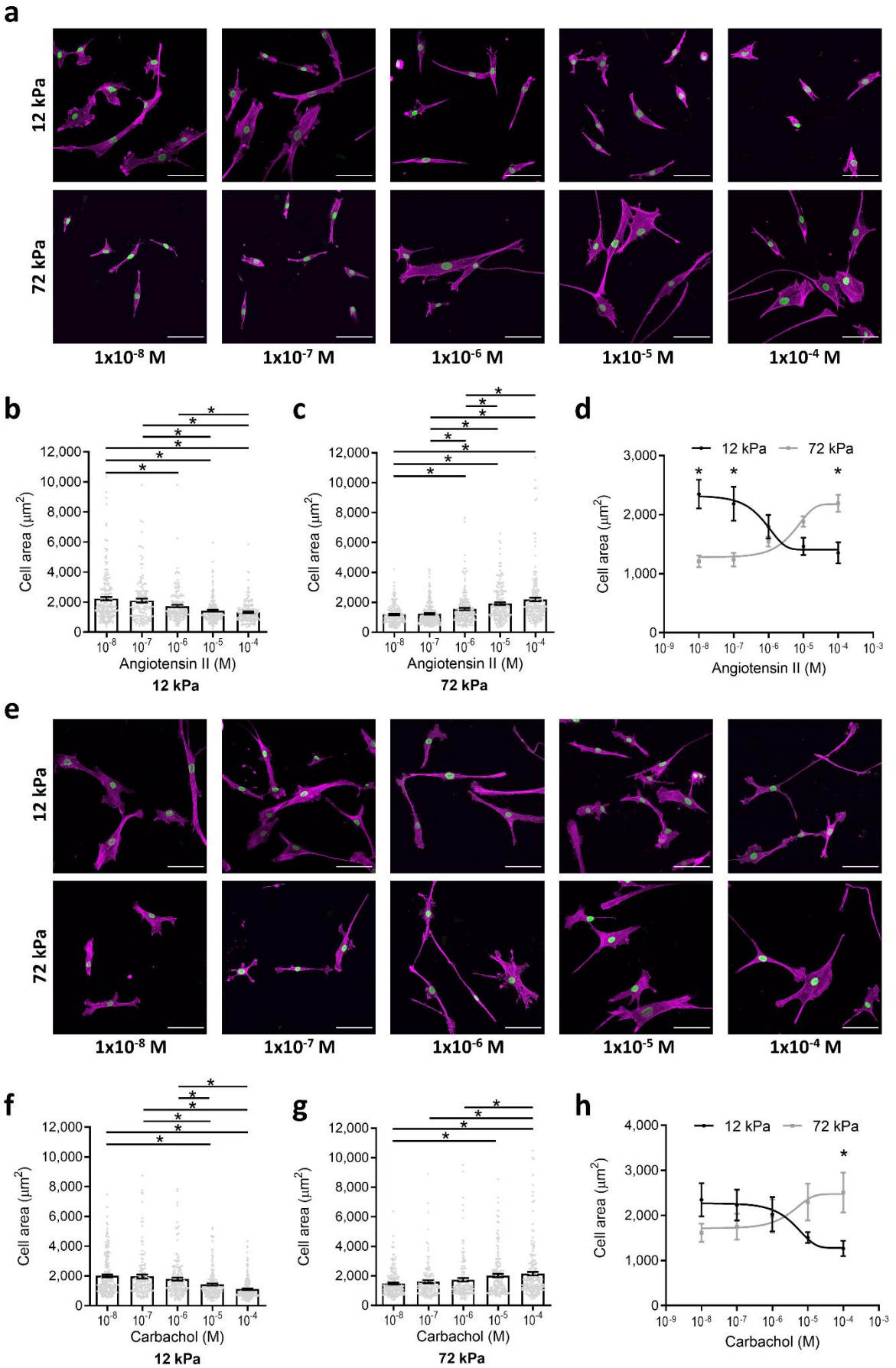
a
12 kPa
72 kPa
1x10-8 M
1x10-7 M
1x10-6 M
1x10-5 M
1x10-4 M
b
c
d
Cell area (μm2)
Angiotensin II (M)
12 kPa
72 kPa
e
f
g
h
Carbachol (M)

Figure 1

Figure 1. VSMC response to contractile agonist stimulation is matrix stiffness dependent. *Representative images of isolated VSMCs cultured on 12 or 72 kPa polyacrylamide hydrogels. Actin cytoskeleton (purple) and Lamin A/C labelled nuclei (green). Scale bar = 100 µm. (a) VSMCs were treated with increasing concentrations of angiotensin II (0.01 – 100 µM) for 30 minutes. VSMC area on (b) 12 kPa and (c) 72 kPa hydrogels representative of 5 independent experiments with ≥158 cells analysed per condition. Significance determined using a one-way ANOVA followed by Tukey's test. (d) Comparison of VSMC response to angiotensin II on 12 and 72 kPa hydrogels. Data is expressed as the mean of the means calculated from 5 independent experiments; significance determined using a two-way ANOVA followed by Sidak's test. (e) VSMCs were treated with increasing concentrations of carbachol (0.01 – 100 µM) for 30 minutes. VSMC area on (f) 12 kPa and (g) 72 kPa hydrogels representative of 5 independent experiments with ≥149 cells analysed per condition. Significance determined using a one-way ANOVA followed by Tukey's test. (h) Comparison of VSMC response to carbachol on 12 and 72 kPa hydrogels. Data is expressed as the mean of the means calculated from 5 independent experiments; significance determined using a two-way ANOVA followed by Sidak's test. (* = $p < 0.05$, error bars represent ± SEM).*

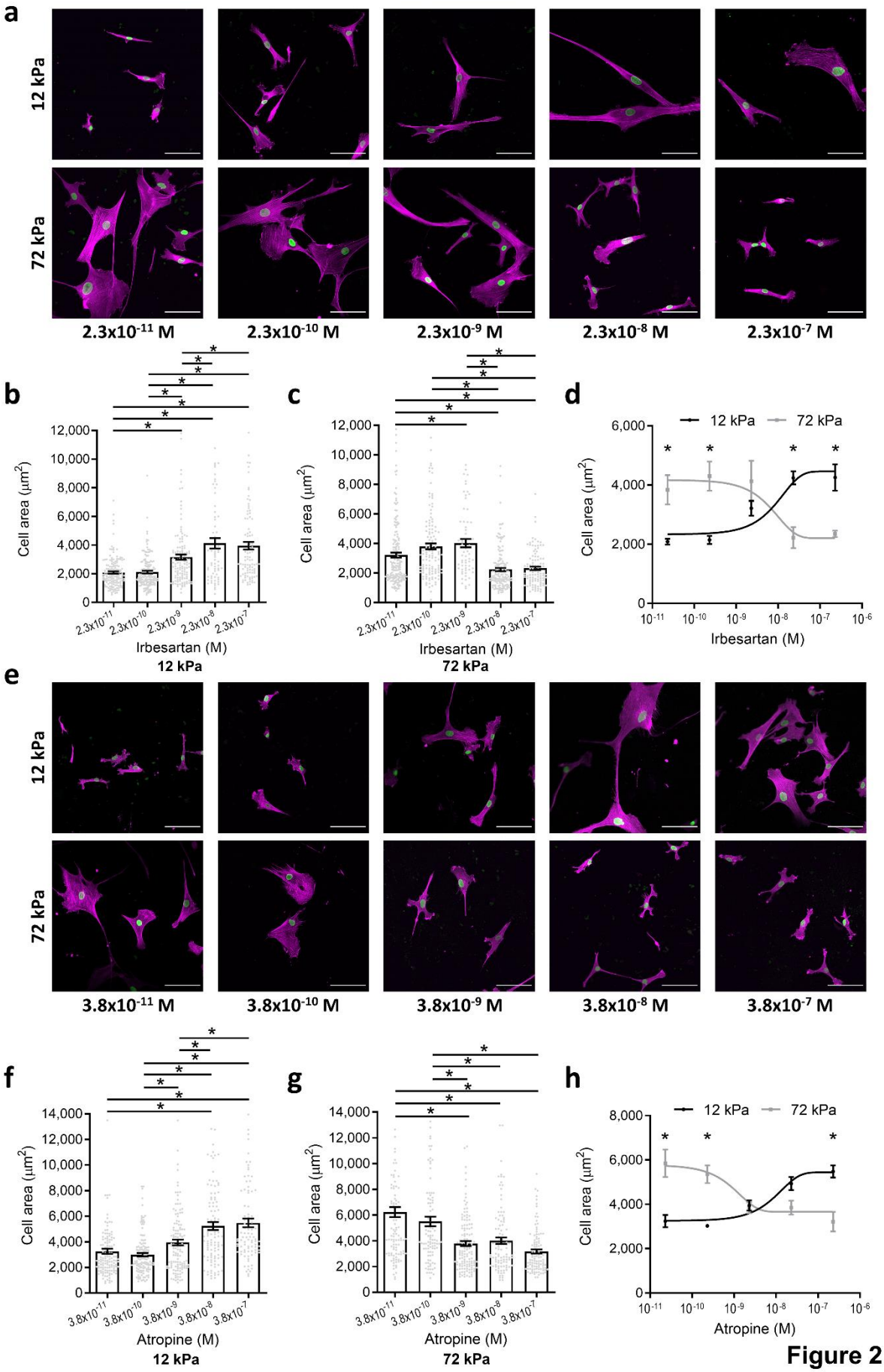
a
12 kPa
72 kPa
2.3x10-11 M
2.3x10-10 M
2.3x10-9 M
2.3x10-8 M
2.3x10-7 M
b
Cell area (µm2)
Irbesartan (M)
12 kPa
c
Irbesartan (M)
72 kPa
d
12 kPa
72 kPa
Irbesartan (M)
e
3.8x10-11 M
3.8x10-10 M
3.8x10-9 M
3.8x10-8 M
3.8x10-7 M
f
Atropine (M)
12 kPa
g
Atropine (M)
72 kPa
h
Atropine (M)

Figure 2

Figure 2. VSMC response to contractile agonist stimulation is blocked by receptor antagonism. *Actin cytoskeleton (purple) and Lamin A/C labelled nuclei (green). Scale bar = 100 µm. (a) Representative images of isolated VSMCs cultured on 12 or 72 kPa polyacrylamide hydrogels treated with angiotensin II (10 µM) for 30 minutes in the presence of increasing concentrations of irbesartan (0.023 – 230 nM). VSMC area on (b) 12 kPa and (c) 72 kPa hydrogels representative of 5 independent experiments with ≥97 cells analysed per condition. Significance determined using a one-way ANOVA followed by Tukey's test. (d) Comparison of VSMC response to angiotensin II in the presence of irbesartan on 12 and 72 kPa hydrogels. Data is expressed as the mean of the means calculated from 5 independent experiments; significance determined using a two-way ANOVA followed by Sidak's test. (e) Representative images of isolated VSMCs cultured on 12 or 72 kPa polyacrylamide hydrogels treated with carbachol (10 µM) for 30 minutes in the presence of increasing concentrations of atropine (0.038 – 380 nM). VSMC area on (f) 12 kPa and (g) 72 kPa hydrogels representative of 5 independent experiments with ≥93 cells analysed per condition. Significance determined using a one-way ANOVA followed by Tukey's test. (h) Comparison of VSMC response to carbachol in the presence of atropine on 12 and 72 kPa hydrogels. Data is expressed as the mean of the means calculated from 5 independent experiments; significance determined using a two-way ANOVA followed by Sidak's test. (* = $p < 0.05$, error bars represent ± SEM).*

3.2 Isolated smooth muscle cells undergo a hypertrophic response on rigid substrates following contractile agonist stimulation.

The above data demonstrates that VSMC response to contractile agonist stimulation is regulated by matrix rigidity. We next sought to determine whether VSMC volume, as well as area was enlarged following contractile agonist stimulation on rigid substrates. Quiescent VSMCs were seeded on pliable and rigid hydrogels and stimulated with angiotensin II. Confocal microscopy was used to measure VSMC volume. As previously observed (Ahmed et al., 2022), VSMCs on pliable hydrogels underwent a contractile response following angiotensin II stimulation, decreasing in cell area but displaying no change in volume (**Figure 3a-c**). In contrast, angiotensin II stimulation of VSMCs on rigid hydrogels resulted in both cell area and volume enlargement, indicative of a hypertrophic response (**Figure 3a-c**). On both rigidities of hydrogel, angiotensin II stimulated VSMCs displayed a positive correlation between cell area and volume (**Figure 3d**). Linear regression revealed that the correlation between VSMC area and volume was similar on both matrices (12 kPa + AngII R^2 = 0.6186, 72 kPa + AngII R^2 = 0.6023) (**Figure 3d**).

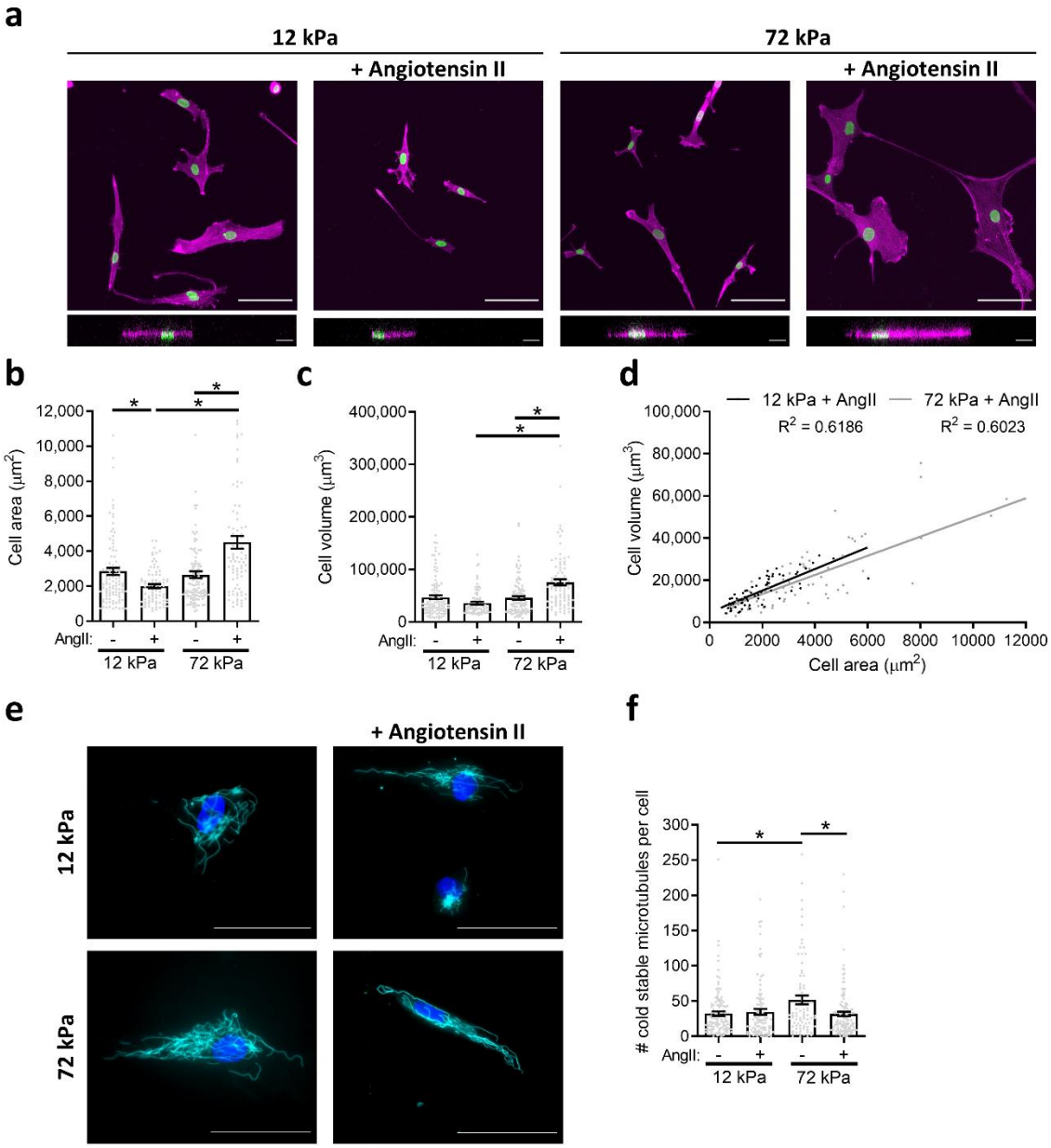

Figure 3. VSMC undergo a hypertrophic response on rigid substrates following angiotensin II stimulation. *(a) Representative images of isolated VSMCs cultured on 12 or 72 kPa polyacrylamide hydrogels treated with angiotensin II (AngII) (10 µM). Actin cytoskeleton (purple) and Lamin A/C labelled nuclei (green). Top – Representative XY images of VSMC area, scale bar = 100 µm. Bottom – Representative XZ images of VSMC height, scale bar = 20 µm. (b) VSMC area and (c) volume, representative of 5 independent experiments with ≥82 cells analysed per condition. Significance determined using a one-way ANOVA followed by Sidak's test. (d) Correlation between area and volume in angiotensin II stimulated VSMCs on 12 and 72 kPa hydrogels. (e) Representative images of isolated VSMCs seeded on 12 or 72 kPa polyacrylamide hydrogels in the presence or absence of AngII (10 µM) stimulation. Cold-stable microtubules, (α-tubulin, aqua) and nuclei (DAPI, blue). Scale bar = 50 µm. (f) number of cold-stable microtubules per cell, representative of 5 independent experiments, with ≥81 cells analysed per condition; significance determined using a two-way ANOVA followed by Sidak's test. (* = $p < 0.05$, error bars represent ± SEM).*

3.3 Extracellular matrix rigidity regulates microtubule stability within isolated smooth muscle cells.

Based on the morphological changes observed above, contractile agonist stimulation promotes VSMC contraction on pliable hydrogels and VSMC hypertrophy on rigid hydrogels. Previous studies have shown that matrix rigidity promotes increased VSMC traction stress generation (Sazonova et al., 2015; Petit et al., 2019). To confirm that angiotensin II stimulated VSMCs seeded on rigid hydrogels generated enhanced traction stresses, we next performed traction force microscopy. Analysis revealed that VSMCs seeded on rigid hydrogels generated greater maximal and total traction stress following angiotensin II stimulation, compared to their counterparts on pliable hydrogels (**Supplementary Figure S1**). As cells generate actomyosin derived traction forces, deformational stresses are also placed upon the cell membrane (Johnson et al., 2021). Microtubules exist in a mechanical balance with actomyosin activity, serving as compression bearing struts capable of resisting actomyosin-generated deformational stresses (Stamenović, 2005; Brangwynne et al., 2006; Johnson et al., 2021). This relationship is defined by the tensegrity model which predicts that microtubule destabilisation will lead to greater actomyosin derived force generation (Stamenović, 2005). As VSMCs on rigid hydrogels generate enhanced traction stresses, we predicted that decreased microtubule stability may contribute to increased traction stress generation. To test this, we performed a cold-stable microtubule assay on isolated VSMCs in the presence or absence of angiotensin II stimulation. Upon exposure to cold temperatures, microtubules readily undergo catastrophe, with only stabilised microtubule filaments remaining. After clearing the tubulin monomers, the number of stabilised microtubules can be counted (Ochoa et al., 2011). On pliable hydrogels, angiotensin II stimulation had no effect on microtubule stability (**Figure 3e & f**). Microtubule stability was found to increase in unstimulated VSMCs that were seeded on rigid compared to pliable substrates (**Figure 3e & f**). However, following angiotensin II stimulation this enhanced stability was lost, with angiotensin II stimulated VSMCs on rigid hydrogels displaying similar levels of microtubule stability as cells on pliable hydrogels (**Figure 3e & f**).

3.4 Microtubule destabilisation promotes isolated smooth muscle cell hypertrophy following contractile agonist stimulation.

The above data shows that on rigid hydrogels, VSMCs stimulated with angiotensin II undergo a hypertrophic response that is accompanied by an increase in traction force generation and a decrease in microtubule stability. We hypothesised that the loss of microtubule stability was driving VSMC hypertrophy on rigid substrates. Quiescent VSMCs were seeded onto pliable and rigid hydrogels and pre-treated with increasing concentrations of microtubule stabilisers prior to angiotensin II stimulation. Treatment with two microtubule stabilisers, paclitaxel or epothilone B, had no effect on the contractile response of VSMCs seeded on pliable hydrogels (**Figure 4a, b, d-f & h**). Meanwhile, increasing concentrations of either microtubule stabiliser was sufficient to prevent the increase in VSMC area observed following angiotensin II stimulation on rigid hydrogels (**Figure 4a, c-e, g & h**).

Given that microtubule stabilisation prevented the enlargement of VSMCs on rigid substrates following angiotensin II stimulation, we then sought to determine whether microtubule destabilisation would have the opposite effect. VSMCs were pre-treated with increasing concentrations of the microtubule destabilisers colchicine or nocodazole, and then stimulated with angiotensin II. On pliable hydrogels, VSMCs treated with either colchicine or nocodazole displayed increased cell area following angiotensin II stimulation (**Figure 5a, b, d-f & h**). In contrast, treatment with the microtubule destabilisers had no effect on VSMCs seeded on rigid hydrogels (**Figure 5a, c-e, g & h**). All microtubule targeting agents were used at concentrations that did not cause cell death, as confirmed through a viability assay for concentrations of epothilone B and nocodazole (**Supplementary Figure S2**) or previously for paclitaxel and colchicine (Ahmed et al., 2022).

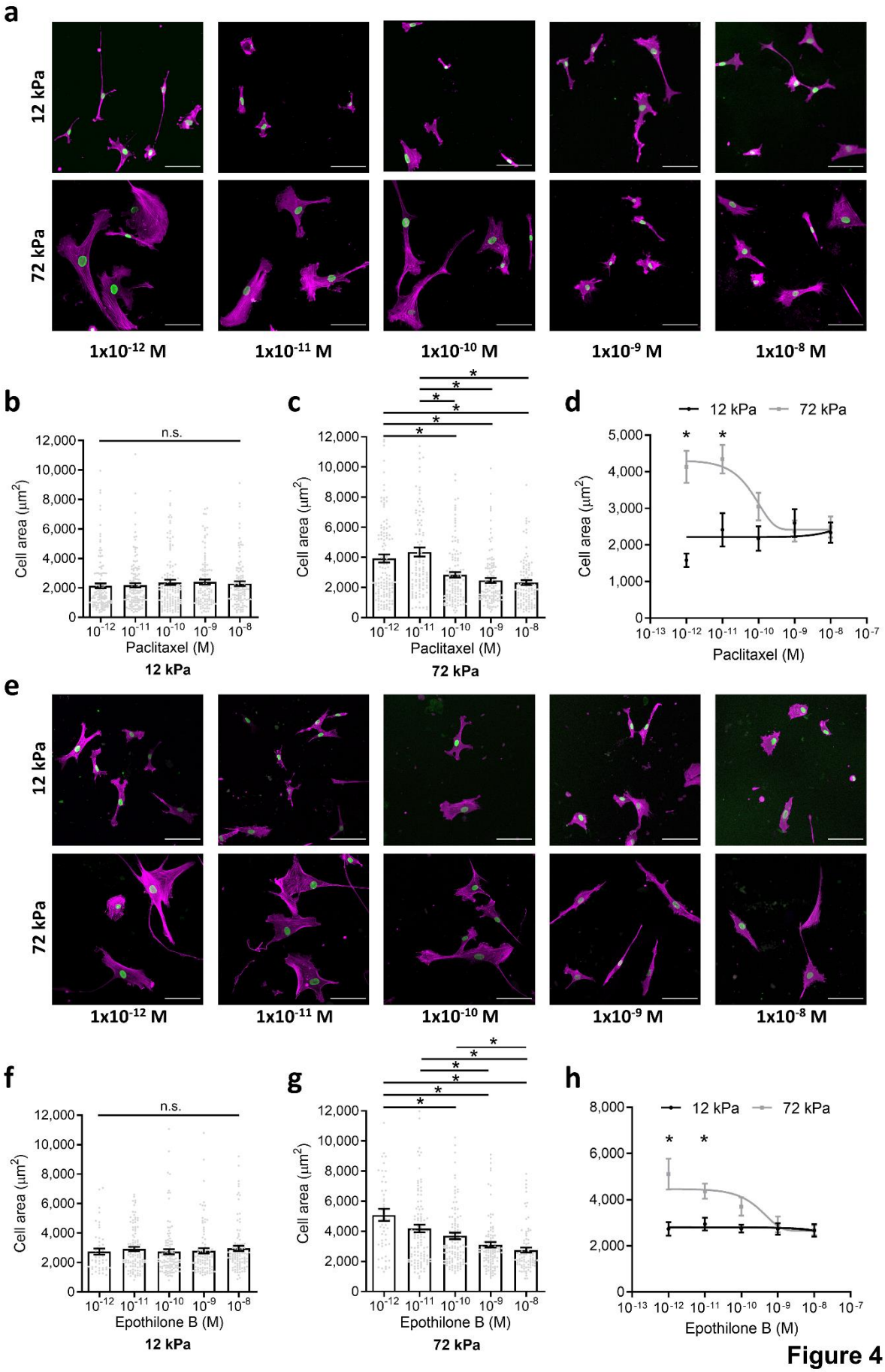
a
12 kPa
72 kPa
1x10-12 M
1x10-11 M
1x10-10 M
1x10-9 M
1x10-8 M
b
n.s.
Cell area (μm2)
Paclitaxel (M)
12 kPa
c
Cell area (μm2)
Paclitaxel (M)
72 kPa
d
12 kPa
72 kPa
Cell area (μm2)
Paclitaxel (M)
e
12 kPa
72 kPa
1x10-12 M
1x10-11 M
1x10-10 M
1x10-9 M
1x10-8 M
f
n.s.
Cell area (μm2)
Epothilone B (M)
12 kPa
g
Cell area (μm2)
Epothilone B (M)
72 kPa
h
12 kPa
72 kPa
Epothilone B (M)

Figure 4

Figure 4. Microtubule stabilisation prevents VSMC enlargement on rigid substrates following angiotensin II stimulation. *Representative images of isolated VSMCs cultured on 12 or 72 kPa polyacrylamide hydrogels stimulated with angiotensin II (10 µM). Actin cytoskeleton (purple) and Lamin A/C labelled nuclei (green). Scale bar = 100 µm. (a) VSMCs were pre-treated with increasing concentrations of paclitaxel (0.001 – 10 nM). VSMC area on (b) 12 kPa and (c) 72 kPa hydrogels representative of 5 independent experiments with ≥100 cells analysed per condition. Significance determined using a one-way ANOVA followed by Tukey's test. (d) Comparison of VSMC response to paclitaxel pre-treatment on 12 and 72 kPa hydrogels. Data is expressed as the mean of the means calculated from 5 independent experiments; significance determined using a two-way ANOVA followed by Sidak's test. (e) VSMCs were pre-treated with increasing concentrations of epothilone B (0.001 – 10 nM). VSMC area on (f) 12 kPa and (g) 72 kPa hydrogels representative of 5 independent experiments with ≥53 cells analysed per condition. Significance determined using a one-way ANOVA followed by Tukey's test. (h) Comparison of VSMC response to epothilone B pre-treatment on 12 and 72 kPa hydrogels. Data is expressed as the mean of the means calculated from 5 independent experiments; significance determined using a two-way ANOVA followed by Sidak's test. (n.s. = non-significant, * = $p < 0.05$, error bars represent ± SEM).*

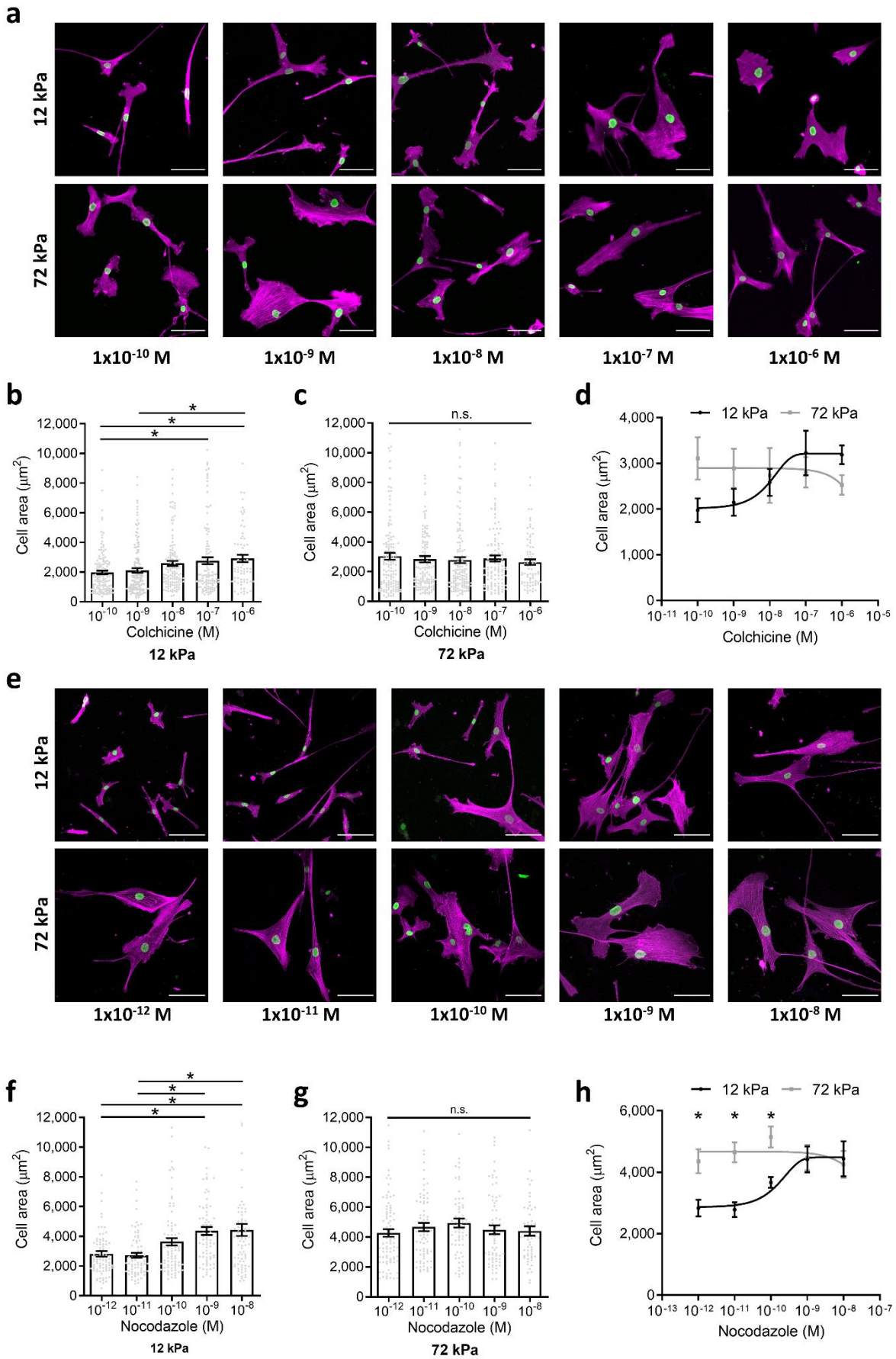
a
12 kPa
72 kPa
1x10-10 M
1x10-9 M
1x10-8 M
1x10-7 M
1x10-6 M
b
Cell area (µm2)
Colchicine (M)
12 kPa
c
n.s.
Colchicine (M)
72 kPa
d
12 kPa
72 kPa
Cell area (µm2)
Colchicine (M)
e
12 kPa
72 kPa
1x10-12 M
1x10-11 M
1x10-10 M
1x10-9 M
1x10-8 M
f
Cell area (µm2)
Nocodazole (M)
12 kPa
g
n.s.
Cell area (µm2)
Nocodazole (M)
72 kPa
h
12 kPa
72 kPa
Cell area (µm2)
Nocodazole (M)

Figure 5

Figure 5. Microtubule destabilisation prevents VSMC contraction on pliable substrates following angiotensin II stimulation. *Representative images of isolated VSMCs cultured on 12 or 72 kPa polyacrylamide hydrogels stimulated with angiotensin II (10 µM). Actin cytoskeleton (purple) and Lamin A/C labelled nuclei (green). Scale bar = 100 µm. (a) VSMCs were pre-treated with increasing concentrations of colchicine (0.1 – 1000 nM). VSMC area on (b) 12 kPa and (c) 72 kPa hydrogels representative of 5 independent experiments with ≥79 cells analysed per condition. Significance determined using a one-way ANOVA followed by Tukey's test. (d) Comparison of VSMC response to paclitaxel pre-treatment on 12 and 72 kPa hydrogels. Data is expressed as the mean of the means calculated from 5 independent experiments; significance determined using a two-way ANOVA followed by Sidak's test. (e) VSMCs were pre-treated with increasing concentrations of nocodazole (0.001 – 10 nM). VSMC area on (f) 12 kPa and (g) 72 kPa hydrogels representative of 5 independent experiments with ≥58 cells analysed per condition. Significance determined using a one-way ANOVA followed by Tukey's test. (h) Comparison of VSMC response to nocodazole pre-treatment on 12 and 72 kPa hydrogels. Data is expressed as the mean of the means calculated from 5 independent experiments; significance determined using a two-way ANOVA followed by Sidak's test. (n.s. = non-significant, * = $p < 0.05$, error bars represent ± SEM).*

Having determined that microtubule stability regulated changes in VSMC area, we next sought to measure changes in VSMC volume and subsequently confirm if microtubule instability was driving the hypertrophic response. Quiescent VSMCs were pre-treated with concentrations of paclitaxel or colchicine that altered both VSMC area (**Figure 4a-d, 5a-d**) and caused a detectable change in the number of cold-stable microtubules (**Supplementary Figure S3**). Following pre-treatment, VSMCs were stimulated with angiotensin II and confocal microscopy was used to assess changes in cell volume. Treatment with the microtubule stabiliser paclitaxel had no effect on the volume of VSMCs seeded on pliable hydrogels (**Figure 6a-c**). In contrast, microtubule stabilisation prevented the angiotensin II induced increase in VSMC volume on rigid hydrogels (**Figure 6a-c**). Meanwhile, microtubule destabilisation, via colchicine pre-treatment, increased VSMC volume on pliable hydrogels following angiotensin II stimulation, indicative of a hypertrophic response. No further increase in VSMC volume following microtubule destabilisation was observed in VSMCs seeded on rigid hydrogels (**Figure 6d-f**).

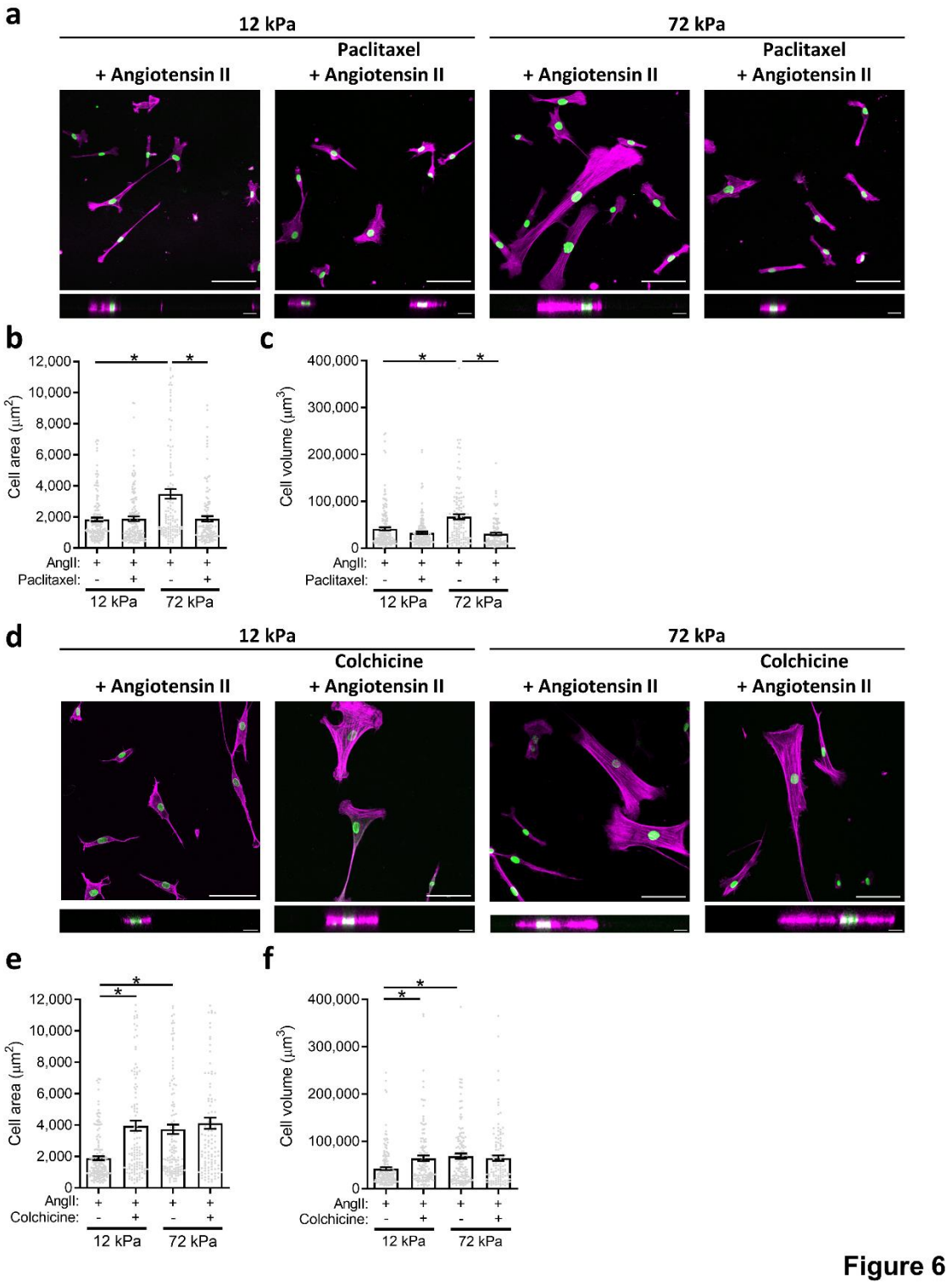

Figure 6. VSMC hypertrophy is regulated by microtubule stability. *Representative images of isolated VSMCs cultured on 12 or 72 kPa polyacrylamide hydrogels stimulated with angiotensin II (AngII) (10 μM). Actin cytoskeleton (purple) and Lamin A/C labelled nuclei (green). Top – Representative XY images of VSMC area, scale bar = 100 μm. Bottom – Representative XZ images of VSMC height, scale bar = 20 μm. (a) Paclitaxel (1 nM) pre-treated VSMCs. (b) VSMC area and (c) volume, representative of 5 independent experiments with ≥114 cells analysed per condition. (d) Colchicine (100 nM) pre-treated VSMCs. (e) VSMC area and (f) volume, representative of 5 independent experiments with ≥113 cells analysed per condition. Significance determined using a one-way ANOVA followed by Sidak's test. (* = $p < 0.05$, error bars represent ± SEM).*

3.5 Extracellular calcium ion influx promotes VSMC hypertrophy on rigid hydrogels

The above data shows that in response to angiotensin II stimulation, VSMCs undergo contraction on pliable hydrogels, but display a hypertrophic response on rigid hydrogels. Angiotensin II mediated activation of the AT1 receptor drives calcium ion (Ca^{2+}) release from the sarcoplasmic reticulum, increasing cytosolic Ca^{2+} levels (Woodrum and Brophy, 2001). Therefore, we next investigated whether ECM rigidity promoted differences in intracellular calcium handling. Quiescent VSMCs were pre-treated with an increasing concentration of either the ryanodine receptor antagonist, dantrolene, or the IP_3 channel blocker, xestospongin C, prior to angiotensin II stimulation. On pliable hydrogels, increasing concentrations of dantrolene or xestospongin C prevented VSMCs from undergoing a contractile response and decreasing in cell area (**Supplementary Figure S4a, b, d-f & h**). Likewise, treatment with dantrolene or xestospongin C prevented the angiotensin II induced enlargement of VSMCs on rigid hydrogels (**Supplementary Figure S4a, c-e, g & h**). Neither compound had any effect on VSMC viability (**Supplementary Figure S5a & b**). This suggests that sarcoplasmic Ca^{2+} release is a common component of both the contractile and hypertrophic response.

ECM rigidity is known to promote the activation of SACs, enabling the influx of extracellular Ca^{2+} in cardiac fibroblasts (Stewart and Turner, 2021). To test whether this was also true in VSMCs, we next utilised the SAC blocker, GsMTx-4. Quiescent VSMCs were pre-treated with an increasing concentration of GsMTx-4 prior to angiotensin II treatment on pliable and rigid hydrogels. Analysis revealed that GsMTx-4 pre-treatment had no effect on VSMC area on pliable hydrogels (**Figure 7a, b & d**). In contrast, GsMTx-4 pre-treatment blocked the increase in VSMC area on rigid hydrogels in a concentration dependent manner (**Figure 7a, c & d**). GsMTx-4 pre-treatment had no effect on the viability of VSMCs (**Supplementary Figure S5c**). To confirm that changes in VSMC area correlated with changes in volume, we next performed confocal microscopy on GsMTx-4 pre-treated VSMCs. SAC blockade had no effect on angiotensin II treated VSMC area or volume on pliable hydrogels (**Figure 7e-f**). However, on rigid hydrogels, GsMTx-4 pre-treatment blocked the angiotensin II induced increases in VSMC area and volume (**Figure 7e-f**).

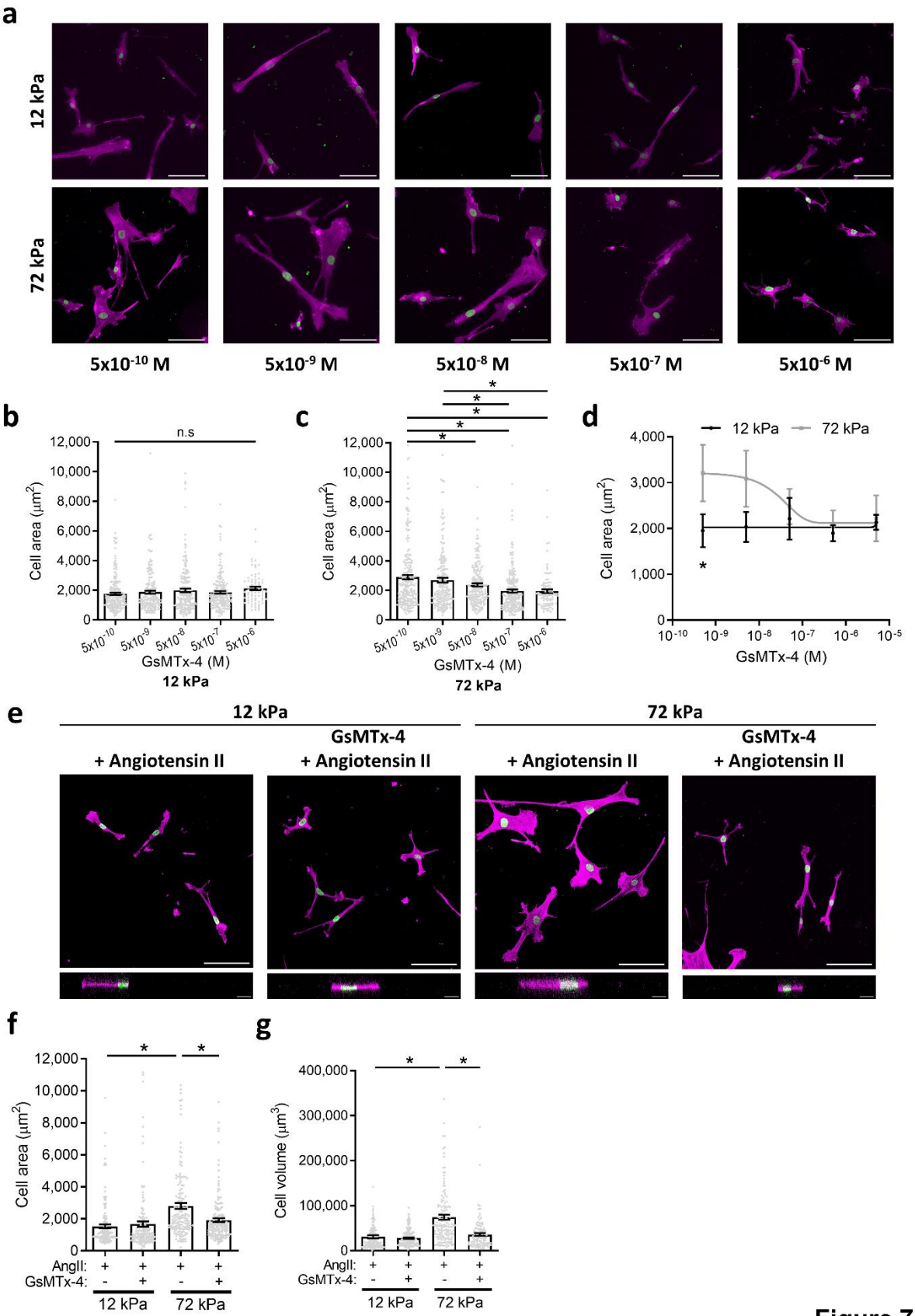
a
12 kPa
72 kPa
5x10-10 M
5x10-9 M
5x10-8 M
5x10-7 M
5x10-6 M
b
n.s
Cell area (µm2)
GsMTx-4 (M)
12 kPa
c
Cell area (µm2)
GsMTx-4 (M)
72 kPa
d
12 kPa
72 kPa
Cell area (µm2)
GsMTx-4 (M)
e
12 kPa
72 kPa
+ Angiotensin II
GsMTx-4
+ Angiotensin II
f
Cell area (µm2)
AngII:
GsMTx-4:
12 kPa
72 kPa
g
Cell volume (µm3)
AngII:
GsMTx-4:
12 kPa
72 kPa

Figure 7

Figure 7. Extracellular calcium influx promotes VSMC hypertrophy on rigid substrates. *Representative images of isolated VSMCs cultured on 12 or 72 kPa polyacrylamide hydrogels stimulated with angiotensin II (AngII) (10 µM). Actin cytoskeleton (purple) and Lamin A/C labelled nuclei (green). (a) VSMCs were pre-treated with increasing concentrations of GsMTx-4 (0.5 – 5000 nM). Scale bar = 100 µm. VSMC area on (b) 12 kPa and (c) 72 kPa hydrogels representative of 5 independent experiments with ≥72 cells analysed per condition. Significance determined using a one-way ANOVA followed by Tukey's test. (d) Comparison of VSMC response to GsMTx-4 pre-treatment on 12 and 72 kPa hydrogels. Data is expressed as the mean of the means calculated from 5 independent experiments; significance determined using a two-way ANOVA followed by Sidak's test. (e) GsMTx-4 (500 nM) pre-treated VSMCs. Top – Representative XY images of VSMC area, scale bar = 100 µm. Bottom – Representative XZ images of VSMC height, scale bar = 20 µm. (f) VSMC area and (g) volume, representative of 5 independent experiments with ≥116 cells analysed per condition. Significance determined using a one-way ANOVA followed by Sidak's test. (* = $p < 0.05$, error bars represent ± SEM).*

3.6 Piezo1-mediated calcium influx destabilises microtubules and drives VSMC hypertrophy

The above data shows that VSMC hypertrophy on rigid substrates is mediated by SAC activation. Piezo1 is a SAC known to be involved in atherosclerosis and abdominal aortic aneurysm mediated VSMC dysfunction (Qian et al., 2022; Yin et al., 2022). Whether piezo1 is involved in VSMC hypertrophy remains unknown. We therefore investigated its potential role in regulating VSMC response to ECM rigidity by utilising an siRNA mediated knockdown approach. Western blotting confirmed that two independent siRNAs efficiently depleted piezo1 in VSMCs (**Figure 8a & b**). Analysis revealed that piezo1 depletion had no effect on angiotensin II induced VSMC contractility on pliable hydrogels, with no change in VSMC area or volume detected. (**Figure 8c-e**). In contrast, piezo1 depletion blocked the angiotensin II mediated increase in VSMC area and volume on rigid hydrogels (**Figure 8c-e**). These data confirm that piezo1 is a novel mediator of VSMC hypertrophy. Finally, we sought to determine if piezo1 activity was driving VSMC hypertrophy through the induction of microtubule instability. To test this idea, we performed cold-stable microtubule assays on VSMCs that were either pre-treated with GsMTx-4 or depleted for piezo1. Analysis revealed that GsMTx-4 mediated SAC blockade (**Figure 9a & b**) or piezo1 depletion (**Figure 9c & d**) restored microtubule stability on VSMCs seeded on rigid hydrogels whilst having no effect on those seeded on pliable hydrogels.

To confirm that Ca^{2+} influx was driving microtubule destabilisation, we performed a cold-stable microtubule assay in the presence or absence of extracellular Ca^{2+}. The absence of extracellular Ca^{2+} had no effect on the number of cold-stable microtubules detected in angiotensin II stimulated VSMCs on pliable hydrogels (**Figure 9e & f**). In contrast, the number of cold-stable microtubules increased within angiotensin II stimulated VSMCs on rigid hydrogels when extracellular Ca^{2+} was absent (**Figure 9e & f**). This suggests that piezo1-mediated Ca^{2+} influx decreases microtubule stability and induces VSMC hypertrophy on rigid hydrogels following angiotensin II stimulation.

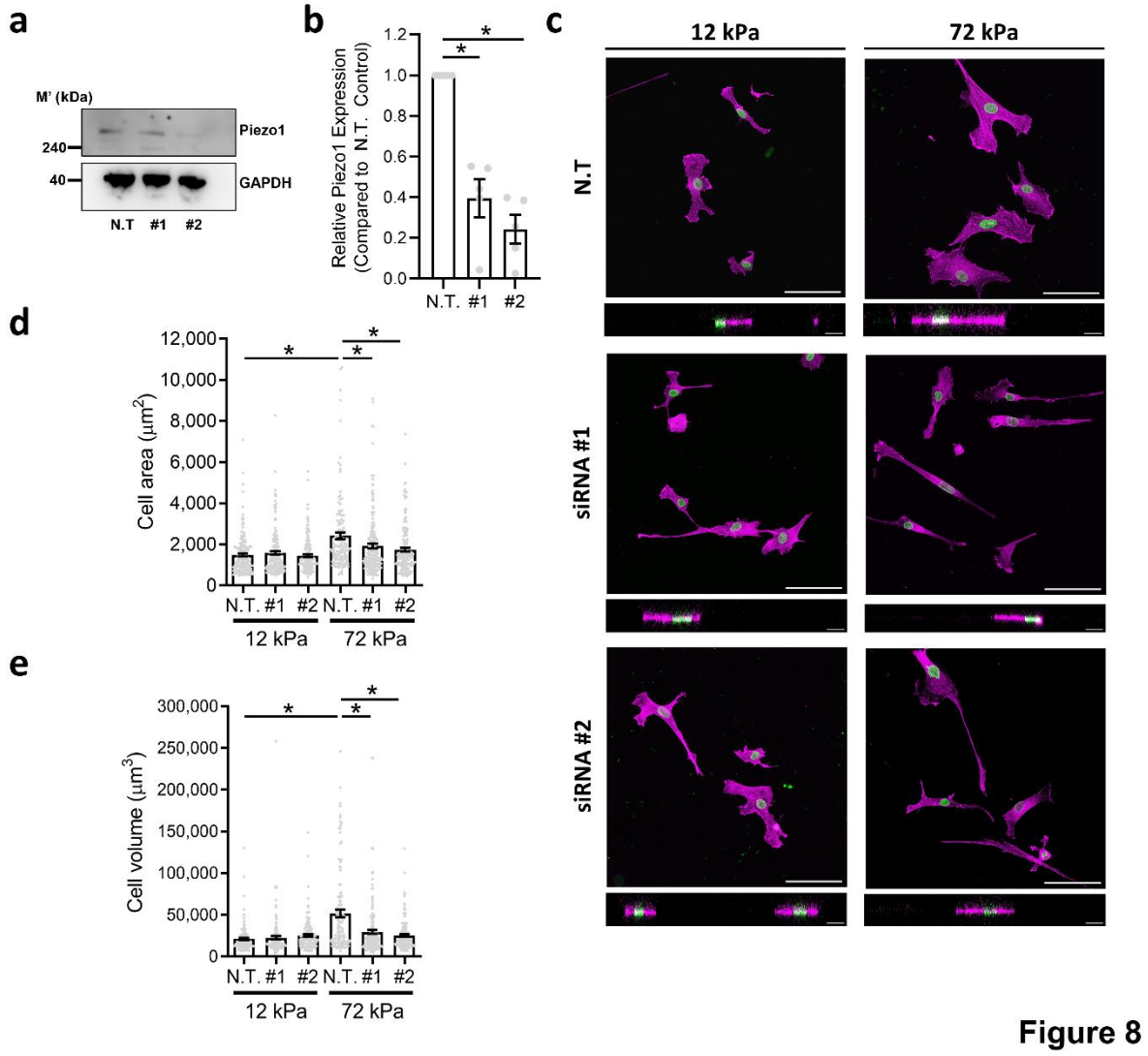

Figure 8. Piezo1 regulates VSMC hypertrophy in response to ECM rigidity. *(a) Representative Western blot and (b) densitometric analysis of siRNA mediated piezo1 depletion. Data representative of 5 independent experiments. Significance determined using a one-way ANOVA followed by Dunnett's test. (c) Representative images of piezo1-depleted VSMCs cultured on 12 or 72 kPa hydrogels following angiotensin II (10 μM) stimulation. N.T. = non-targeting siRNA. Actin cytoskeleton (purple) and Lamin A/C labelled nuclei (green). Top – Representative XY images of VSMC area, scale bar = 100 μm. Bottom – Representative XZ images of VSMC height, scale bar = 20 μm. (d) VSMC area and (e) volume, representative of 5 independent experiments with ≥120 cells analysed per condition. Significance determined using a one-way ANOVA followed by Sidak's test. (* = $p < 0.05$, error bars represent ± SEM).*

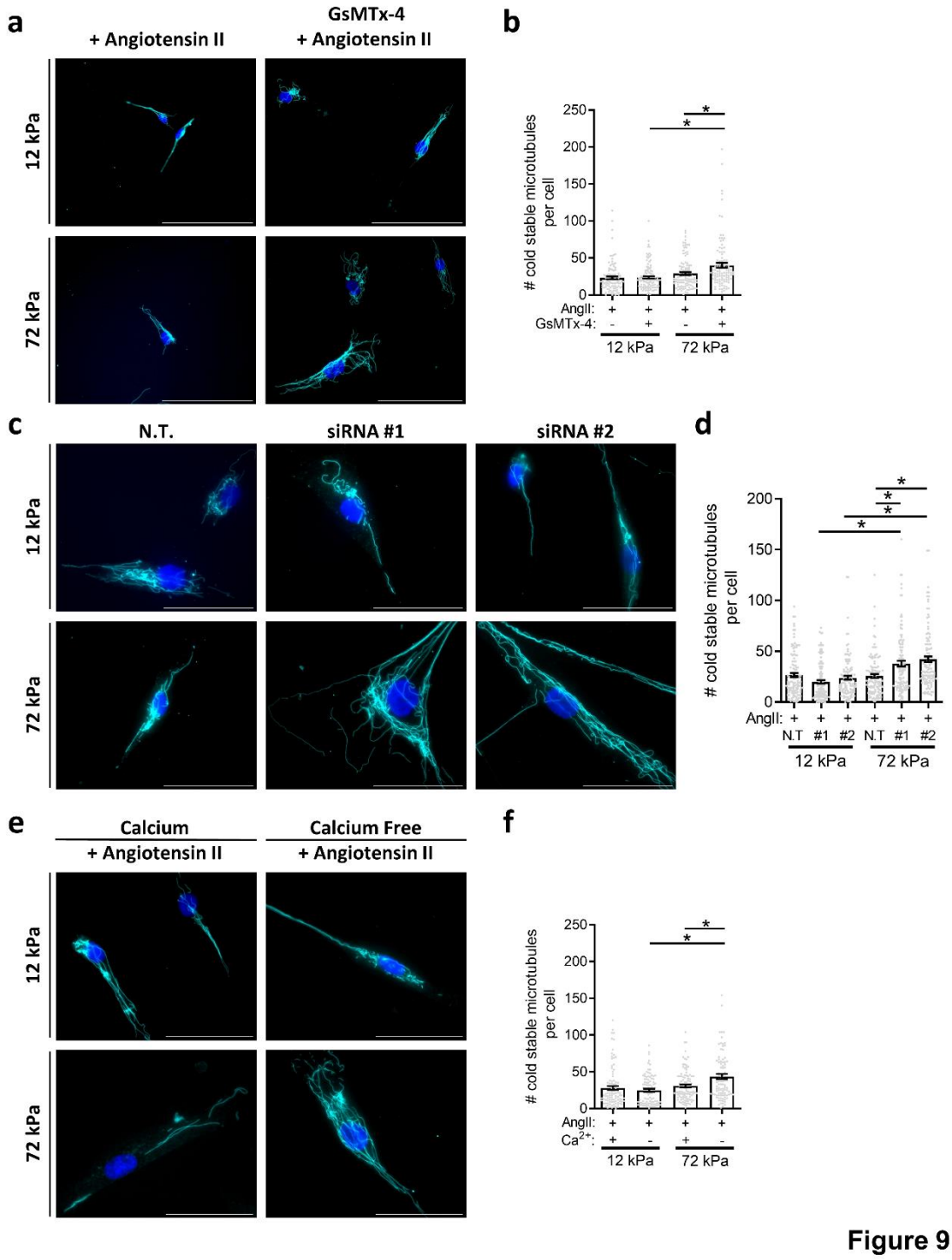

Figure 9. Extracellular calcium influx via Piezo1 ion channels triggers microtubule destabilisation. *Representative images of isolated VSMCs cultured on 12 or 72 kPa polyacrylamide hydrogels treated with angiotensin II (10 µM). Cold-stable microtubules, (α-tubulin, aqua) and nuclei (DAPI, blue). Scale bar = 50 µm. (a) GsMTx-4 (500 nM) pre-treated VSMCs. (b) number of cold-stable microtubules per cell, representative of 5 independent experiments, with ≥100 cells analysed per condition. (c) siRNA-mediated piezo1 depleted VSMCs. N.T. = non-targeting siRNA. (d) number of cold-stable microtubules per cell, representative of 5 independent experiments, with ≥109 cells analysed per condition. (e) VSMCs were cultured in the presence or absence of extracellular calcium (f) number of cold-stable microtubules per cell, representative of 5 independent experiments, with ≥98 cells analysed per condition. Significance determined using a one-way ANOVA followed by Sidak's test. (* = $p < 0.05$, error bars represent ± SEM).*

4. Discussion

Our understanding of the mechanisms driving VSMC dysfunction and its contribution to decreased aortic compliance in ageing and CV disease remains limited. Progress has been hindered by a lack of easy to use, *in vitro* tools through which pathological mechanisms can be investigated. In this study, we utilised polyacrylamide hydrogels whose rigidity (pliable 12 kPa, rigid 72 kPa) mimicked the respective stiffness of healthy and aged/diseased aortic walls (Hayenga et al., 2011; Tracqui et al., 2011; Minaisah et al., 2016; Rezvani-Sharif et al., 2019). Polyacrylamide hydrogels are biologically inert and can be easily fabricated to a specific rigidity in-house, using generic research equipment and skills (Kandow et al., 2007; Caliari and Burdick, 2016; Minaisah et al., 2016; Mohammed et al., 2019). This makes them ideal substrates for investigating how ECM rigidity regulates cellular function. Previous studies have shown that ECM rigidity promotes the dedifferentiation of VSMCs, downregulating contractile markers whilst increasing the expression of proliferative genes (Brown et al., 2010; Sazonova et al., 2015; Nagayama and Nishimiya, 2020). Increased VSMC migration, adhesion and proliferation have also been reported (Wong et al., 2003; Brown et al., 2010; Sazonova et al., 2015; Nagayama and Nishimiya, 2020; Rickel et al., 2020). Furthermore, in response to matrix rigidity, VSMC reorganise their actin cytoskeleton and generate enhanced traction stresses, a finding we recapitulate in this study (Brown et al., 2010; Sazonova et al., 2015; Petit et al., 2019; Sanyour et al., 2019). We now show that contractile agonist stimulation of quiescent VSMCs on pliable (healthy) or rigid (aged/diseased) matrices results in a differential response; VSMCs on pliable matrices decreased in area as they undergo contraction, whereas increased cell area was observed in VSMCs on rigid matrices. Furthermore, on rigid matrices, contractile agonist stimulation also promoted an increase in VSMC volume. These findings suggest that changes in VSMC morphology following contractile agonist stimulation are differentially regulated on pliable and rigid matrices. On pliable matrices, actomyosin activity drives contraction and VSMC area subsequently decreases but volume remains unchanged. In contrast, on rigid matrices, changes in VSMC morphology are driven by enhanced volume. Importantly, we identify for the first time that enhanced matrix rigidity initiates a hypertrophic response within VSMCs, akin to that seen *in vivo* in response to hypertension (Owens and Schwartz, 1983; Rizzoni et al., 2000; Zhang et al., 2005; Schiffrin, 2012).

Hypertension is regarded as one of the strongest risk factors for the progression of CV disease (Kjeldsen, 2018). VSMCs dedifferentiate as a result of hypertension, becoming dysfunctional and hypertrophic (Touyz et al., 2018). VSMC hypertrophy contributes to aortic wall thickening, increased aortic stiffness and reduced aortic compliance, which in turn leads to hypertension (Brown et al., 2018). The causality between VSMC hypertrophy and hypertension is cyclic in nature, with the development of one promoting the onset of the other. Current methods of investigating VSMC hypertrophy generally utilise animal models, including rat models of hypertension and genetic depletion in mice (Owens and Schwartz, 1983; Hixon et al., 2000; Choi et al., 2019; Bai et al., 2021). We now show that the *in vitro* induction of VSMC hypertrophy can be achieved through culturing cells on rigid matrices. This enables the mechanisms regulating VSMC hypertrophy and the potential of anti-hypertrophic compounds to be investigated at a greater throughput whilst using a less invasive and more ethical method. Importantly, we correlated increased VSMC area following angiotensin II

stimulation with an increase in VSMC volume. This enabled us to predict potential beneficial or deleterious effects of pharmacological agents on VSMC hypertrophy, prior to confirming those predictions through 3-dimensional confocal microscopy. Through this method, we identified novel regulators of VSMC hypertrophy using physiologically or pathologically relevant ECM rigidities.

In hypertension, VSMC Ca^{2+} handling is known to become dysregulated, with VSMCs entering a hypercontractile state that further increases aortic rigidity whilst simultaneously reducing aortic compliance (Touyz et al., 2018). Our findings suggest that the internal release of Ca^{2+} from the sarcoplasmic reticulum, following angiotensin II stimulation, is unperturbed by increased ECM rigidity. Instead, VSMC hypertrophy is driven by the extracellular influx of Ca^{2+} through mechanosensitive SACs. Specifically, we identify piezo1 as a driver of ECM rigidity induced VSMC hypertrophy. VSMC piezo1 expression is upregulated in mouse models of atherosclerosis and abdominal aortic aneurysms, with dysregulation of VSMC mechanosensation shown to drive these disease states (Qian et al., 2022; Yin et al., 2022). Furthermore, reduced aortic compliance is observed in both atherosclerosis and abdominal aortic aneurysms (Glasser et al., 1997; Mitchell et al., 2010; Lacolley et al., 2017). Enhanced VSMC actomyosin force generation is known to contribute to reduced aortic compliance with inhibition of actomyosin activity resulting in reduced aortic wall rigidity (Qiu et al., 2010). Our study now suggests that VSMC hypertrophy may also contribute to the increased aortic wall rigidity observed in ageing and CV disease. Furthermore, we identify piezo1 as a critical driver of VSMC hypertrophy in response to increased ECM rigidity. Pharmacological blockade of piezo1, may prove beneficial and could form part of a potential therapeutic strategy to reduce VSMC hypertrophy, decrease aortic wall rigidity and restore aortic compliance. Further research to test these findings in *ex vivo* settings is an essential next step in confirming the validity of our findings.

VSMC response to increased actomyosin-derived force generation on rigid hydrogels is predicted by the tensegrity model. In this model, microtubules serve as compression bearing struts that resist actomyosin generated strain (Johnson et al., 2021). Healthy VSMC behaviour is therefore a balance between microtubule stability and actomyosin activity; actomyosin activity drives VSMC contraction while the microtubules maintain VSMC morphology and protect against strain induced cellular damage (Stamenović, 2005; Brangwynne et al., 2006). The tensegrity model also predicts that microtubule destabilisation results in increased traction stress generation, a hypothesis previously confirmed by both wire myography and traction force microscopy (Paul et al., 2000; Zhang et al., 2000; Platts et al., 2002; Ahmed et al., 2022). We show that the tensegrity model drives VSMC hypertrophy on rigid matrices, where angiotensin II stimulation triggers microtubule destabilisation. Importantly, treatment with microtubule stabilising agents blocked VSMC hypertrophy on rigid matrices whilst maintaining VSMC contractility on pliable matrices. This suggests that therapeutic pathways that promote microtubule stabilisation may be a potential novel approach to target VSMC hypertrophy specifically in areas of aortic stiffness. Current antihypertensive therapies target the renin-angiotensin system and either prevent the production of angiotensin II or block the activation of the AT1 receptor (Hernández-

Hernández et al., 2002). Whilst these therapies are effective and well tolerated, they target healthy and dysfunctional VSMCs alike.

Whilst microtubule stabilisation blocked VSMC hypertrophy, treatment with microtubule destabilising agents had the opposite effect and induced VSMC hypertrophy on pliable matrices. Colchicine, a microtubule destabilising agent, is currently being researched for its CV benefits. Colchicine treatment has been experimentally shown to protect against endothelial cell dysfunction (Huang et al., 2014; Kajikawa et al., 2019; Zălar et al., 2022), reduce VSMC proliferation and migration *in vitro* (Zhang et al., 2022), and supress atherosclerotic plaque development in some animal models (Martínez et al., 2018). However, wire myography and traction force microscopy both show that colchicine treatment also increases VSMC isomeric force generation (Zhang et al., 2000; Platts et al., 2002; Ahmed et al., 2022), suggesting that colchicine treatment will increase aortic wall rigidity and decrease aortic compliance. VSMC hypertrophy may subsequently be an unwanted side effect of any potential colchicine therapy.

Our data suggest that microtubule stability serves as a hypertrophic switch, in VSMCs destabilisation promotes hypertrophy, whereas stabilisation blocks hypertrophy. Previous studies have shown that microtubule catastrophe can be driven by increased levels of cytosolic Ca^{2+} (O'Brien et al., 1997; Thompson et al., 2014). In this study, we identify that on rigid matrices, angiotensin II stimulation of VSMCs leads to an influx of Ca^{2+} through mechanosensitive piezo1 channels. Blocking the influx of Ca^{2+} maintains microtubule stability and in turn prevents VSMC hypertrophy. These findings pave the wave for confirmatory studies in *ex vivo* and *in vivo* models. Furthermore, through comparing the response of VSMCs on pliable and rigid matrices we not only identify potential anti-hypertrophic targets, but also identify side effects of proposed therapies for the treatment of CV and other diseases. Although we have established a role for piezo1 and microtubule stability in regulating VSMC hypertrophy, further research is required to elucidate the molecular mechanisms through which ECM rigidity drives this response and how Ca^{2+} regulates microtubule stability. Developing a better understanding of the connection between Ca^{2+} and microtubule stability will enhance our mechanistic understanding of VSMC hypertrophy and will likely identify further targets that have the therapeutic potential to restore aortic compliance in ageing and CV disease.

References

Ahmed, S., Johnson, Robert.T., Solanki, R., Afewerki, T., Wostear, F., and Warren, Derek.T. (2022). Using Polyacrylamide Hydrogels to Model Physiological Aortic Stiffness Reveals that Microtubules Are Critical Regulators of Isolated Smooth Muscle Cell Morphology and Contractility. Frontiers in Pharmacology *13*: 836710.

Ahmed, S., and Warren, D.T. (2018). Vascular smooth muscle cell contractile function and mechanotransduction. Vessel Plus *2*: 36.

Atkinson, S.J., Gontarczyk, A.M., Alghamdi, A.A., Ellison, T.S., Johnson, R.T., Fowler, W.J., et al. (2018). The β3-integrin endothelial adhesome regulates microtubule-dependent cell migration. EMBO Rep *19*: e44578.

Bai, L., Kee, H.J., Choi, S.Y., Seok, Y.M., Kim, G.R., Kee, S.-J., et al. (2021). HDAC5 inhibition reduces angiotensin II-induced vascular contraction, hypertrophy, and oxidative stress in a mouse model. Biomedicine & Pharmacotherapy *134*: 111162.

Brangwynne, C.P., MacKintosh, F.C., Kumar, S., Geisse, N.A., Talbot, J., Mahadevan, L., et al. (2006). Microtubules can bear enhanced compressive loads in living cells because of lateral reinforcement. Journal of Cell Biology *173*: 733–741.

Brown, I.A.M., Diederich, L., Good, M.E., DeLalio, L.J., Murphy, S.A., Cortese-Krott, M.M., et al. (2018). Vascular Smooth Muscle Remodeling in Conductive and Resistance Arteries in Hypertension. Arteriosclerosis, Thrombosis, and Vascular Biology *38*: 1969–1985.

Brown, X.Q., Bartolak-Suki, E., Williams, C., Walker, M.L., Weaver, V.M., and Wong, J.Y. (2010). Effect of substrate stiffness and PDGF on the behavior of vascular smooth muscle cells: implications for atherosclerosis. J Cell Physiol *225*: 115–122.

Caliari, S.R., and Burdick, J.A. (2016). A practical guide to hydrogels for cell culture. Nat Methods *13*: 405–414.

Choi, S.Y., Kee, H.J., Sun, S., Seok, Y.M., Ryu, Y., Kim, G.R., et al. (2019). Histone deacetylase inhibitor LMK235 attenuates vascular constriction and aortic remodelling in hypertension. Journal of Cellular and Molecular Medicine *23*: 2801–2812.

Curtis, M.J., Alexander, S., Cirino, G., Docherty, J.R., George, C.H., Giembycz, M.A., et al. (2018). Experimental design and analysis and their reporting II: updated and simplified guidance for authors and peer reviewers. British Journal of Pharmacology *175*: 987–993.

Glasser, S.P., Arnett, D.K., McVeigh, G.E., Finkelstein, S.M., Bank, A.J., Morgan, D.J., et al. (1997). Vascular Compliance and Cardiovascular Disease: A Risk Factor or a Marker? American Journal of Hypertension *10*: 1175–1189.

Hayashi, K., and Naiki, T. (2009). Adaptation and remodeling of vascular wall; biomechanical response to hypertension. Journal of the Mechanical Behavior of Biomedical Materials *2*: 3–19.

Hayenga, H.N., Trache, A., Trzeciakowski, J., and Humphrey, J.D. (2011). Regional atherosclerotic plaque properties in ApoE-/- mice quantified by atomic force, immunofluorescence, and light microscopy. J Vasc Res *48*: 495–504.

Hernández-Hernández, R., Sosa-Canache, B., Velasco, M., Armas-Hernández, M.J., Armas-Padilla, M.C., and Cammarata, R. (2002). Angiotensin II receptor antagonists role in arterial hypertension. J Hum Hypertens *16*: S93–S99.

Hixon, M.L., Muro-Cacho, C., Wagner, M.W., Obejero-Paz, C., Millie, E., Fujio, Y., et al. (2000). Akt1/PKB upregulation leads to vascular smooth muscle cell hypertrophy and polyploidization. J Clin Invest *106*: 1011–1020.

Huang, C., Cen, C., Wang, C., Zhan, H., and Ding, X. (2014). Synergistic effects of colchicine combined with atorvastatin in rats with hyperlipidemia. Lipids Health Dis *13*: 67.

Johnson, R.T., Solanki, R., and Warren, D.T. (2021). Mechanical programming of arterial smooth muscle cells in health and ageing. Biophys Rev *13*: 757–768.

Kajikawa, M., Higashi, Y., Tomiyama, H., Maruhashi, T., Kurisu, S., Kihara, Y., et al. (2019). Effect of short-term colchicine treatment on endothelial function in patients with coronary artery disease. International Journal of Cardiology *281*: 35–39.

Kandow, C.E., Georges, P.C., Janmey, P.A., and Beningo, K.A. (2007). Polyacrylamide Hydrogels for Cell Mechanics: Steps Toward Optimization and Alternative Uses. In Methods in Cell Biology, (Academic Press), pp 29–46.

Kjeldsen, S.E. (2018). Hypertension and cardiovascular risk: General aspects. Pharmacological Research *129*: 95–99.

Kobayashi, T., and Sokabe, M. (2010). Sensing substrate rigidity by mechanosensitive ion channels with stress fibers and focal adhesions. Current Opinion in Cell Biology *22*: 669–676.

Lacolley, P., Regnault, V., and Laurent, S. (2020). Mechanisms of Arterial Stiffening. Arteriosclerosis, Thrombosis, and Vascular Biology *40*: 1055–1062.

Lacolley, P., Regnault, V., Segers, P., and Laurent, S. (2017). Vascular Smooth Muscle Cells and Arterial Stiffening: Relevance in Development, Aging, and Disease. Physiological Reviews *97*: 1555–1617.

Leloup, A.J.A., Van Hove, C.E., De Moudt, S., De Meyer, G.R.Y., De Keulenaer, G.W., and Fransen, P. (2019). Vascular smooth muscle cell contraction and relaxation in the isolated aorta: a critical regulator of large artery compliance. Physiological Reports *7*: e13934.

Liu, S., and Lin, Z. (2022). Vascular Smooth Muscle Cells Mechanosensitive Regulators and Vascular Remodeling. JVR *59*: 90–113.

Lowis, C., Winaya, A., Kumari, P., Rivera, C., Vlahos, J., Hermantara, R., et al. (2023). Mechanosignals in abdominal aortic aneurysms. Frontiers in Cardiovascular Medicine *9*: 1021934.

Martínez, G.J., Celermajer, D.S., and Patel, S. (2018). The NLRP3 inflammasome and the emerging role of colchicine to inhibit atherosclerosis-associated inflammation. Atherosclerosis *269*: 262–271.

Minaisah, R.-M., Cox, S., and Warren, D.T. (2016). The Use of Polyacrylamide Hydrogels to Study the Effects of Matrix Stiffness on Nuclear Envelope Properties. In The Nuclear Envelope, S. Shackleton, P. Collas, and E.C. Schirmer, eds. (New York, NY: Springer New York), pp 233–239.

Mitchell, G.F., Hwang, S.-J., Vasan, R.S., Larson, M.G., Pencina, M.J., Hamburg, N.M., et al. (2010). Arterial Stiffness and Cardiovascular Events. Circulation *121*: 505–511.

Mohammed, D., Versaevel, M., Bruyère, C., Alaimo, L., Luciano, M., Vercruysse, E., et al. (2019). Innovative Tools for Mechanobiology: Unraveling Outside-In and Inside-Out Mechanotransduction. Frontiers in Bioengineering and Biotechnology *7*: 162.

Nagayama, K., and Nishimiya, K. (2020). Moderate substrate stiffness induces vascular smooth muscle cell differentiation through cellular morphological and tensional changes. Biomed Mater Eng *31*: 157–167.

Nourse, J.L., and Pathak, M.M. (2017). How cells channel their stress: Interplay between Piezo1 and the cytoskeleton. Seminars in Cell & Developmental Biology *71*: 3–12.

O'Brien, E.T., Salmon, E. d., and Erickson, H.P. (1997). How calcium causes microtubule depolymerization. Cell Motility *36*: 125–135.

Ochoa, C.D., Stevens, T., and Balczon, R. (2011). Cold exposure reveals two populations of microtubules in pulmonary endothelia. Am J Physiol Lung Cell Mol Physiol *300*: L132–L138.

Owens, G.K., and Schwartz, S.M. (1983). Vascular smooth muscle cell hypertrophy and hyperploidy in the Goldblatt hypertensive rat. Circulation Research *53*: 491–501.

Paul, R.J., Bowman, P.S., and Kolodney, M.S. (2000). Effects of microtubule disruption on force, velocity, stiffness and [Ca2+]i in porcine coronary arteries. American Journal of Physiology-Heart and Circulatory Physiology *279*: H2493–H2501.

Petit, C., Guignandon, A., and Avril, S. (2019). Traction Force Measurements of Human Aortic Smooth Muscle Cells Reveal a Motor-Clutch Behavior. Molecular and Cellular Biomechanics.

Platts, S.H., Martinez-Lemus, L.A., and Meininger, G.A. (2002). Microtubule-Dependent Regulation of Vasomotor Tone Requires Rho-Kinase. JVR *39*: 173–182.

Porter, L., Minaisah, R.-M., Ahmed, S., Ali, S., Norton, R., Zhang, Q., et al. (2020). SUN1/2 Are Essential for RhoA/ROCK-Regulated Actomyosin Activity in Isolated Vascular Smooth Muscle Cells. Cells *9*: 132.

Qian, W., Hadi, T., Silvestro, M., Ma, X., Rivera, C.F., Bajpai, A., et al. (2022). Microskeletal stiffness promotes aortic aneurysm by sustaining pathological vascular smooth muscle cell mechanosensation via Piezo1. Nat Commun *13*: 512.

Qiu, H., Zhu, Y., Sun, Z., Trzeciakowski, J.P., Gansner, M., Depre, C., et al. (2010). Short Communication: Vascular Smooth Muscle Cell Stiffness As a Mechanism for Increased Aortic Stiffness With Aging. Circulation Research *107*: 615–619.

Ragnauth, C.D., Warren, D.T., Liu, Y., McNair, R., Tajsic, T., Figg, N., et al. (2010). Prelamin A Acts to Accelerate Smooth Muscle Cell Senescence and Is a Novel Biomarker of Human Vascular Aging. Circulation *121*: 2200–2210.

Rezvani-Sharif, A., Tafazzoli-Shadpour, M., and Avolio, A. (2019). Progressive changes of elastic moduli of arterial wall and atherosclerotic plaque components during plaque development in human coronary arteries. Med Biol Eng Comput *57*: 731–740.

Rickel, A.P., Sanyour, H.J., Leyda, N.A., and Hong, Z. (2020). Extracellular Matrix Proteins and Substrate Stiffness Synergistically Regulate Vascular Smooth Muscle Cell Migration and Cortical Cytoskeleton Organization. ACS Appl. Bio Mater. *3*: 2360–2369.

Rizzoni, D., Porteri, E., Guefi, D., Piccoli, A., Castellano, M., Pasini, G., et al. (2000). Cellular Hypertrophy in Subcutaneous Small Arteries of Patients With Renovascular Hypertension. Hypertension *35*: 931–935.

Safar, M.E., Henry, O., and Meaume, S. (2002). Aortic Pulse Wave Velocity: An Independent Marker of Cardiovascular Risk. The American Journal of Geriatric Cardiology *11*: 295–304.

Sanyour, H.J., Li, N., Rickel, A.P., Childs, J.D., Kinser, C.N., and Hong, Z. (2019). Membrane cholesterol and substrate stiffness co-ordinate to induce the remodelling of the cytoskeleton and the alteration in the biomechanics of vascular smooth muscle cells. Cardiovasc Res *115*: 1369–1380.

Sazonova, O.V., Isenberg, B.C., Herrmann, J., Lee, K.L., Purwada, A., Valentine, A.D., et al. (2015). Extracellular matrix presentation modulates vascular smooth muscle cell mechanotransduction. Matrix Biology *41*: 36–43.

Sazonova, O.V., Lee, K.L., Isenberg, B.C., Rich, C.B., Nugent, M.A., and Wong, J.Y. (2011). Cell-Cell Interactions Mediate the Response of Vascular Smooth Muscle Cells to Substrate Stiffness. Biophysical Journal *101*: 622–630.

Schiffrin, E.L. (2012). Vascular Remodeling in Hypertension. Hypertension *59*: 367–374.

Schindelin, J., Arganda-Carreras, I., Frise, E., Kaynig, V., Longair, M., Pietzsch, T., et al. (2012). Fiji: an open-source platform for biological-image analysis. Nat Methods *9*: 676–682.

Sehgel, N.L., Sun, Z., Hong, Z., Hunter, W.C., Hill, M.A., Vatner, D.E., et al. (2015a). Augmented Vascular Smooth Muscle Cell Stiffness and Adhesion When Hypertension Is Superimposed on Aging. Hypertension *65*: 370–377.

Sehgel, N.L., Vatner, S.F., and Meininger, G.A. (2015b). “Smooth Muscle Cell Stiffness Syndrome”—Revisiting the Structural Basis of Arterial Stiffness. Frontiers in Physiology *6*:.

Sehgel, N.L., Zhu, Y., Sun, Z., Trzeciakowski, J.P., Hong, Z., Hunter, W.C., et al. (2013). Increased vascular smooth muscle cell stiffness: a novel mechanism for aortic stiffness in hypertension. American Journal of Physiology-Heart and Circulatory Physiology *305*: H1281–H1287.

Sequí-Domínguez, I., Cavero-Redondo, I., Álvarez-Bueno, C., Pozuelo-Carrascosa, D.P., Nuñez de Arenas-Arroyo, S., and Martínez-Vizcaíno, V. (2020). Accuracy of Pulse Wave Velocity Predicting Cardiovascular and All-Cause Mortality. A Systematic Review and Meta-Analysis. Journal of Clinical Medicine *9*: 2080.

Stamenović, D. (2005). Microtubules may harden or soften cells, depending of the extent of cell distension. Journal of Biomechanics *38*: 1728–1732.

Stewart, L., and Turner, N.A. (2021). Channelling the Force to Reprogram the Matrix: Mechanosensitive Ion Channels in Cardiac Fibroblasts. Cells *10*: 990.

Thompson, G.L., Roth, C.C., Dalzell, D.R., Kuipers, M.A., and Ibey, B.L. (2014). Calcium influx affects intracellular transport and membrane repair following nanosecond pulsed electric field exposure. JBO *19*: 055005.

Touyz, R.M., Alves-Lopes, R., Rios, F.J., Camargo, L.L., Anagnostopoulou, A., Arner, A., et al. (2018). Vascular smooth muscle contraction in hypertension. Cardiovascular Research *114*: 529–539.

Tracqui, P., Broisat, A., Toczek, J., Mesnier, N., Ohayon, J., and Riou, L. (2011). Mapping elasticity moduli of atherosclerotic plaque in situ via atomic force microscopy. J Struct Biol *174*: 115–123.

Tsamis, A., Krawiec, J.T., and Vorp, D.A. (2013). Elastin and collagen fibre microstructure of the human aorta in ageing and disease: a review. Journal of The Royal Society Interface *10*: 20121004.

Tseng, Q., Duchemin-Pelletier, E., Deshiere, A., Balland, M., Guillou, H., Filhol, O., et al. (2012). Spatial organization of the extracellular matrix regulates cell–cell junction positioning. PNAS *109*: 1506–1511.

Warren, D.T., Tajsic, T., Porter, L.J., Minaisah, R.M., Cobb, A., Jacob, A., et al. (2015). Nesprin-2-dependent ERK1/2 compartmentalisation regulates the DNA damage response in vascular smooth muscle cell ageing. Cell Death Differ *22*: 1540–1550.

Wong, J.Y., Velasco, A., Rajagopalan, P., and Pham, Q. (2003). Directed Movement of Vascular Smooth Muscle Cells on Gradient-Compliant Hydrogels. Langmuir *19*: 1908–1913.

Woodrum, D.A., and Brophy, C.M. (2001). The paradox of smooth muscle physiology. Molecular and Cellular Endocrinology *177*: 135–143.

Yin, Q., Zang, G., Li, N., Sun, C., and Du, R. (2022). Agonist-induced Piezo1 activation promote mitochondrial-dependent apoptosis in vascular smooth muscle cells. BMC Cardiovasc Disord *22*: 287.

Zălar, D.-M., Pop, C., Buzdugan, E., Kiss, B., Ştefan, M.-G., Ghibu, S., et al. (2022). Effects of Colchicine in a Rat Model of Diet-Induced Hyperlipidemia. Antioxidants *11*: 230.

Zhang, D., Jin, N., Rhoades, R.A., Yancey, K.W., and Swartz, D.R. (2000). Influence of microtubules on vascular smooth muscle contraction. J Muscle Res Cell Motil *21*: 293–300.

Zhang, F., He, Q., Qin, C.H., Little, P.J., Weng, J., and Xu, S. (2022). Therapeutic potential of colchicine in cardiovascular medicine: a pharmacological review. Acta Pharmacol Sin *43*: 2173–2190.

Zhang, Y., Griendling, K.K., Dikalova, A., Owens, G.K., and Taylor, W.R. (2005). Vascular Hypertrophy in Angiotensin II–Induced Hypertension Is Mediated by Vascular Smooth Muscle Cell–Derived H2O2. Hypertension *46*: 732–737.

Zhong, Q., Hu, M.-J., Cui, Y.-J., Liang, L., Zhou, M.-M., Yang, Y.-W., et al. (2018). Carotid–Femoral Pulse Wave Velocity in the Prediction of Cardiovascular Events and Mortality: An Updated Systematic Review and Meta-Analysis. Angiology *69*: 617–629.

Zieman, S.J., Melenovsky, V., and Kass, D.A. (2005). Mechanisms, Pathophysiology, and Therapy of Arterial Stiffness. Arteriosclerosis, Thrombosis, and Vascular Biology *25*: 932–943.